Spectral statistics of multiparametric Gaussian ensembles with chiral symmetry

Triparna Mondal and Pragya Shukla
Department of Physics, Indian Institute of Technology, Kharagpur 721302, West Bengal, India

(Received 31 March 2020; accepted 1 September 2020; published 18 September 2020)

The statistics of chiral matrix ensembles with uncorrelated but multivariate Gaussian distributed elements is intuitively expected to be driven by many parameters. Contrary to intuition, however, our theoretical analysis reveals the existence of a single parameter, a function of all ensemble parameters, which governs the dynamics of spectral statistics. The analysis not only extends the formulation (known as complexity parameter formulation) for Hermitian ensembles without chirality to those with it but also reveals the underlying connection between chiral complex systems with seemingly different system conditions as well as between other complex systems, e.g., multiparametric Wishart ensembles as well as generalized Calogero-Sutherland Hamiltonians.

DOI: 10.1103/PhysRevE.102.032131

I. INTRODUCTION

For systems in which the relevant behavior is governed by a linear operator, it is useful to consider the matrix representation in a symmetry preserving basis which in turn puts the constraints on the type of matrix elements and/or structure of the matrix [1–3] (referred to as matrix constraints). The underlying complexity in real systems, however, often manifests through fluctuations of physical properties making it necessary to consider their statistical behavior [4–6]. This in turn requires an analysis of not only single matrices but also their ensemble, with the latter's choice sensitive to the system specific conditions, e.g., hopping range, dimensionality, and boundary conditions; the conditions on the choice of ensemble, i.e., its parameters as well as nature of randomness, are referred to as ensemble constraints. The latter can conspire with matrix constraints in multiple ways to give rise to different types of statistical behavior. This motivates the present paper, in which the primary focus is to analyze the influence of a specific *matrix constraint*, namely, chiral symmetry, on the statistical behavior of complex systems with varying *ensemble constraints,* e.g., disorder [2]. The motivation comes not only from the fundamental aspect of the topic but also from a range of applications in which complexity appears hand in hand with chirality, e.g., charge transport in graphene [7], spectral fluctuations in QCD Dirac operators [8,9], conductance fluctuations in mesoscopic systems [1,10], and topological systems [11–14].

Consider a complex system with chiral symmetry described by an ensemble of chiral Hermitian matrices. For special cases in which the complexity subjects the matrix elements to independent and identical distributions (e.g., cases with ergodic dynamics in the basis space), thus resulting in a minimum number of ensemble constraints, the system can then be represented by a basis-invariant chiral ensemble, e.g., a chiral Gaussian ensemble invariant under orthogonal, unitary, or symplectic transformation (referred to as Ch-GOE, Ch-GUE, and Ch-GSE, respectively) [4–6,8]. For generic cases, however, the information about inhomogeneity of system conditions appears through ensemble parameters (e.g., those with localized dynamics in basis space), and as a consequence an appropriate ensemble representation depends on many of them. Any variation of the system conditions changes the ensemble parameters, thus leading to a multiparametric evolution of the matrix ensemble (in a fixed basis), and it is natural to wonder whether any universality classes can be identified during nonequilibrium stages. As revealed by previous studies, the answer is in the affirmative at least in the case of the multiparametric, nonchiral, Hermitian ensembles (of real-symmetric, complex Hermitian, or real-quaternion matrices); the reasoning is based on a common mathematical formulation of their statistical properties in which ensemble details enter only through a single function of all distribution parameters. Using the function, referred to as the complexity parameter, the nonchiral ensembles can be mapped to a single parametric Brownian ensemble of corresponding symmetry class (real, complex Hermitian, or real-quaternion matrices) [15–20]. The latter can be described as an ensemble of Hermitian matrices $H = H_0 + \sqrt{Y}\,V$, with H_0 taken from one of the stationary ensembles of Hermitian matrices, subjected to perturbation V taken from another stationary ensemble, and Y as the perturbation parameter [21–23]. The mapping not only reveals the underlying universality among nonequilibrium (nonstationary or basis-dependent) Hermitian ensembles but also helps the application of all available information for the latter to the former. A similar formulation in the case of chiral Hermitian matrices is very desirable as well as intuitively expected but is not technically obvious; this is because their off-diagonal blocks are in general non-Hermitian. This motivates us to analyze the multiparametric Gaussian ensembles of chiral Hermitian matrices with and without time-reversal symmetry and seek a single parametric formulation of their spectral and strength (i.e., eigenfunction) fluctuations. As discussed below, the diffusion equation for the ensemble density [joint probability density function (JPDF) of the matrix elements] in terms of the complexity parameter turns out to

be analogous to that of a chiral Brownian ensemble (Ch-BE), a perturbed stationary chiral ensemble with its diffusion governed by the perturbation parameter [24]; a direct diagonalization of the diffusion equation then leads to analogous diffusion equations for the spectral as well as strength statistical measures. Some of the fluctuation measures for the Ch-BE are theoretically analyzed in [24], with their formulation expressed in terms of the perturbation parameter. By replacing the latter by the complexity parameter, the information can then directly be used for the multiparametric Gaussian ensembles of chiral Hermitian matrices.

The implications of the single parametric formulation of the statistics for the multiparametric chiral ensembles are many; e.g., it reveals (i) an analogy among the statistics of different complex systems, represented by the ensembles of different ensemble constraints but the same matrix constraints; (ii) an analogy of the statistics of a complex system for different system conditions; (iii) the connection to a variant of the Calogero-Sutherland Hamiltonian (CSH), thus providing further evidence supporting the claim that the CSH is the hidden backbone Hamiltonian of the world of complex systems [25]; and (iv) the possibility of a similar formulation for multiparametric Wishart ensembles. The importance of these connections as well as the implications makes it necessary to verify our theoretical predictions and is the primary focus of the present paper. For this purpose, we numerically analyze the spectral statistics of the four Gaussian chiral ensembles with different functional dependence of the distribution parameters.

The paper is organized as follows. Section II describes the diffusion of the multiparametric probability density of the chiral ensemble under consideration and presents the complexity parametric formulation of its diffusion when the ensemble parameters (a few or all) are varied. As the steps are essentially the same as in the nonchiral case discussed in [16], we avoid repetition here and only mention the diffusion equation for the ensemble density. An exact diagonalization of the latter then leads to complexity parameter driven diffusion equations for the joint probability distribution functions of the eigenvalues and eigenfunctions. The relevant steps are described in Sec. III; here again we mention only those steps which are different from the nonchiral cases. The numerical analysis presented in Sec. IV verifies our theoretical predictions. We conclude in Sec. V with a brief summary of our results and open questions.

II. MULTIPARAMETRIC GAUSSIAN ENSEMBLES WITH CHIRALITY AND HERMITIAN CONSTRAINTS

A. Matrix representation

A $(2N+\nu)\times(2N+\nu)$ Hermitian matrix with chirality constraint can be described as

$$H=\begin{pmatrix}0 & C\\ C^{\dagger} & 0\end{pmatrix}, \tag{1}$$

where C is a general $N\times(N+\nu)$ complex matrix if H has no other antiunitary symmetry; as clear from above, $H_{k,N+l}=C_{kl}$ [1,2,4,5]. For cases with time-reversal symmetry also present, C is a real or quaternion matrix based on the presence or absence of rotational symmetry (i.e., integer or half integer angular momentum). For clarity purposes, here we confine our study only to C real or complex with no other matrix constraints. The elements of the C matrix can then be written as $C_{kl}=\sum_{s=1}^{\beta}(i)^{s-1}C_{kl;s}$ where $k=1\to N$, $l=1\to(N+\nu)$, and $\beta=1$ or 2 for C real or complex. (The generalization to quaternion C can be done following similar steps but is technically tedious and is therefore not included here.)

B. Diffusion of matrix elements: Ensemble complexity parameter

Using Eq. (1), the distribution, say $\rho(H)$, of the elements of the matrix H can be expressed in terms of those of C:

$$\rho(H)=\rho_c(\{H_{k,N+l}\})\;F_c\;F_h \tag{2}$$

with $\rho_c(C)$ as the probability density of the ensemble of C matrices and with F_c and F_h as the constraints due to chirality and Hermiticity of H, respectively: $F_c=\prod_{k,l=1}^{N}\delta(H_{kl})$ and $F_h(H)=\delta(H-H^{\dagger})$.

For simple presentation of our formulation, here we consider elements of C as independent Gaussian distributed, with arbitrary mean and variances:

$$\rho_c(C;h,b)=\mathcal{N}\exp\left[-\sum_{k,l,s}\frac{1}{2h_{kl;s}}(C_{kl;s}-b_{kl;s})^2\right] \tag{3}$$

with $\sum_{k,l,s}\equiv\sum_{k=1}^{N}\sum_{l=1}^{N+\nu}\sum_{s=1}^{\beta}$ and $\mathcal{N}$ as a normalization constant. Here $h\equiv[h_{kl,s}]$ and $b\equiv[b_{kl,s}]$ refer to the matrices of variances and mean values of $C_{kl;s}$. Clearly, with different choices of h and b matrices, Eq. (3) can give rise to many chiral ensembles; some of them are used below in Sec. IV for numerical verification of our results.

Using $H_{k,N+l}=C_{kl}$, Eq. (3) leads to the ensemble density $\rho(H)$ of the H matrix:

$$\rho(H;h,b)=\mathcal{N}\exp\left[-\sum_{k,l,s}\frac{1}{2h_{kl;s}}(H_{k(N+l)}-b_{kl;s})^2\right]F_c\;F_h. \tag{4}$$

We now consider a diffusive dynamics in the ensemble space of C matrices by a smooth variation of the parameters $h_{kl;s}$ and $b_{kl;s}$. As the dynamics occurs in C-matrix space, it preserves the chirality of H. Proceeding as discussed in [17,19] for the nonchiral case, it can be shown that the diffusion depends on the multiple parameters $h_{kl;s}$ and $b_{kl;s}$ only through a function Y, the latter referred to as the ensemble complexity parameter, if the matrix basis preserves the global constraints on the system. The single parametric evolution of $\rho_c(C)$ can be described as

$$\frac{\partial\rho_c}{\partial Y}=\sum_{k,l,s}\frac{\partial}{\partial C_{kl;s}}\left[\frac{\partial\rho_c}{\partial C_{kl;s}}+\gamma\;C_{kl;s}\;\rho_c\right] \tag{5}$$

with

$$Y=-\frac{1}{2M\gamma}\ln\left[\prod_{k,l}{}'\prod_{s=1}^{\beta}|x_{kl;s}|\;|b_{kl;s}|^2\right]+\text{const} \tag{6}$$

where $x_{kl;s}=1-2\;\gamma\;h_{kl;s}$ and $\prod_{k,l}'$ implies a product over nonzero $x_{kl;s}$ and $b_{kl;s}$, with M as their total number [for example, for the case with all $x_{kl;s}\neq 0$ but $b_{kl;s}=0$, we have

$M = \beta N(N+\nu)$, and, for the case with all $x_{kl;s} \neq 0$ and $b_{kl;s} \neq 0$, we have $M = 2\beta N(N+\nu)$]. Further γ is an arbitrary parameter, related to the final state of the ensemble (giving the variance of matrix elements at the end of the evolution), and the constant in Eq. (6) is determined by the initial state of the ensemble.

Substitution of $C_{kl;s} = H_{kN+l;s}$ in the above then leads to the evolution equation for $\rho(H)$:

$$\frac{\partial \rho}{\partial Y} = \sum_{k,l,s} \frac{\partial}{\partial H_{kN+l;s}} \left[\frac{\partial \rho}{\partial H_{kN+l;s}} + \gamma \, H_{kN+l;s} \, \rho \right]. \tag{7}$$

Equation (7) describes the diffusion of $\rho(H)$ with a finite drift, starting from an arbitrary initial condition, say $\rho_0(H, Y_0)$ at $Y = Y_0$, and approaching the steady limit of CH-GOE or CH-GUE as $Y \to \infty$. With system information in Eq. (7) appearing only through Y, its solution $\rho(H|H_0)$ remains the same for different ensembles, irrespective of the details of h and b matrices, if they share the same Y value and are subjected to the same global constraints. The latter condition can be explained as follows. A generic transformation maps M independent variables (i.e., sets h and b) to another set $\{Y, Y_2, \ldots, Y_M\}$ of independent variables: $h_{kl;s} = h_{kl;s}(Y, Y_2, \ldots, Y_M)$ and $b_{kl;s} = b_{kl;s}(Y, Y_2, \ldots, Y_M)$. This transforms $\rho(h, b) \to \rho(Y, Y_2, \ldots, Y_M)$. Equation (7) describes the Y-governed evolution of ρ while Y_j, $j = 2 \to M$ remain constant. As discussed in [2,17], these $M-1$ constants can be chosen in terms of the basis constants and initial conditions if the basis (chosen to represent H) is kept unchanged during the evolution. The statistics during the transition is then governed by Y only with Y_j, $j = 2 \to M$ appearing as the constants of evolution. For analysis of physical properties, it is important to choose a physically motivated basis. For comparison of ensembles subjected to the same global constraints, the appropriate basis is the one which preserves these constraints. This in turn ensures the same evolution constants Y_j, $j = 2 \to M$ as well as a common initial state for the ensembles under consideration (the related examples for nonchiral cases are discussed in [2,16,17] and can be generalized for chiral ones).

In [17], a similar diffusion equation of the matrix elements confined by harmonic potential and governed by a single parameter was also derived for the nonchiral Hermitian ensemble of multiparametric Gaussian ensembles (also see [19] for an alternative approach). Equation (7) is different from its nonchiral counterparts only in terms of the distinct matrix elements which appear in the equation: the former has contributions only from the elements in one off-diagonal block C (or $C^\dagger$) of the H matrix while the latter has it from all off-diagonals.

A Ch-BE is a special case of the multiparametric chiral Gaussian ensembles [its ensemble parameters are the same as given in Eq. (18) for the chiral Rosenzweig-Porter ensemble (Ch-RPE)]. The equation governing evolution of the matrix elements of Ch-BE is derived in [24] [see Eq. (32) therein] and is analogous, as expected, to Eq. (7). Various statistical measures for the former are also discussed in [24] and, as discussed below, can directly be applied to the multiparametric chiral Gaussian ensembles following the analogy.

III. SPECTRAL STATISTICS

With H given by Eq. (1), let E be its eigenvalue matrix ($E_{mn} = e_n \delta_{mn}$) and U the eigenvector matrix, with U_{kn} as the kth component of the eigenvector U_n corresponding to eigenvalue e_n. Following from Eq. (1), Tr(H) is zero, which then implies that the eigenvalues of H exist in equal and opposite pairs or are zero; let us refer to such pairs as e_n, e_{n+N} with $e_n = -e_{n+N}$, $1 \leqslant n \leqslant N$. Clearly, with E as the $(2N+\nu) \times (2N+\nu)$ diagonal matrix, the number of zero eigenvalues is ν. Henceforth, the eigenvalues are labeled such that e_k, $k = 1 \to N$ correspond to positive eigenvalues with their negative counterparts lying at $k = N+1 \to 2N$, and $k = 2N+1 \to 2N+\nu$ refers to zero eigenvalues.

A variation of system conditions perturbs H, resulting in dynamics of the matrix elements and thereby of the eigenvalues and eigenfunctions. The latter's response to change in H can be derived from the eigenvalue equation $HU = UE$ along with the unitary condition $U^\dagger U = I_{2N+\nu}$; this has been discussed in detail for nonchiral cases in many previous studies [15,17–20] and in [24] for the chiral Brownian ensemble. Although the intermediate steps in chiral cases are essentially similar to the nonchiral ones, their final responses turn out to be different. The difference mainly arises from the response of the pairwise symmetric eigenvalues, chirality induced relations between eigenfunction components, as well as existence of zero modes in a chiral matrix. As the present paper is confined to the spectral fluctuation analysis, we include chiral spectral responses in Appendix A to make the presentation self-contained.

A. Joint probability distribution of eigenvalues

As in the nonchiral case [15,20], an exact diagonalization of Eq. (7) leads to the diffusion equations for the eigenvalues and eigenfunctions. These equations can also be obtained by standard second order perturbation theory for Hermitian matrices with chiral symmetry. With primary focus on the eigenfunction statistics, the perturbation route was used in [24] in the case of Ch-BEs [24]. This route, however, is based on H expressed as the sum of two matrices (the elements of one matrix subjected to perturbation by the other, which in turn manifests as perturbation of one stationary ensemble by another), and its application to the multiparametric case (where the parameters of a single ensemble are subjected to perturbation) is not directly obvious. It is therefore instructive to consider the exact diagonalization route too (it also gives insights about how the dynamics of ρ in the matrix space is mimicked by that in the parameter space).

Let us define $P(E) \equiv P(e_1, e_2, \ldots, e_{2N+\nu})$ as the JPDF of the eigenvalues e_i, $i = 1, 2, \ldots, 2N+\nu$ of H:

$$P(e_1, e_2, \ldots, e_{2N+\nu}) \equiv P_N(e_1, e_2, \ldots, e_N) \prod_{k=1}^{N} \delta(e_k + e_{k+N}) \times \prod_{n=1}^{\nu} \delta(e_{2N+n}) \tag{8}$$

with $P_N(E) \equiv P_N(e_1, e_2, \ldots, e_N)$ as the JPDF of the N nonzero positive eigenvalues. As discussed in Appendix B, an exact integration of Eq. (7) leads to Y governed evolution of P_N described by the following equation:

$$\frac{\partial P_N}{\partial Y} = 2\sum_{n=1}^{N} \frac{\partial}{\partial e_n}\left[\frac{\partial}{\partial e_n} - \beta\left(\frac{\nu+1/2}{e_n} + \sum_{m=1}^{N}\frac{2e_n}{e_n^2 - e_m^2}\right) + \gamma e_n\right] P_N. \tag{9}$$

(As the derivation is essentially similar to that of nonchiral cases discussed in [15,17], we avoid repeating the intermediate steps here but include them in Appendix B.) The above equation describes the diffusion of $P_N(E, Y)$, with a finite drift, from an arbitrary initial state $P_N(E_0, Y_0)$ at $Y = Y_0$. In limit $\frac{\partial P_N}{\partial Y} \to 0$ or $Y \to \infty$, the diffusion approaches a unique steady state: $P_N(E; \infty) = C_\beta\ |Q_N|^\beta$ with C_β as the normalization constant and

$$|Q_N|^\beta = \prod_{m<n=1}^{N} \left|e_m^2 - e_n^2\right|^\beta \prod_{k=1}^{N} |e_k|^{\beta(\nu+1/2)} \exp\left[-\frac{\gamma}{2}\sum_{k=1}^{N} e_k^2\right]. \tag{10}$$

It is desirable to seek the solution of Eq. (9) for finite Y. This is, however, technically difficult, requires a separate study, and is also beyond the purview of the present paper, where our main objective is to numerically confirm the validity of complexity parametric formulation of the spectral statistics. Important insights in the latter can, however, be obtained by the following analogy: Eq. (9) for the multiparametric case is analogous to that of Ch-BE [24] [this is as expected, following the analogy of Eq. (7) with evolution of the ensemble density of a Ch-BE]. Consequently, the theoretical results, obtained in [24], for the statistics of chiral Brownian ensembles can directly be used for the multiparametric chiral Gaussian ensembles. For example, following the same steps as discussed in [24], the diffusion equation for $P_N(E, Y)$ can be rewritten in terms of the Schrödinger equation for the general state $\Psi(E, Y) = \frac{P_N(E,Y)}{|Q|^{\beta/2}}$ of a variant of the CSH of the interacting particles (with eigenvalues now playing the role of particles). The ground state and many of the excited states of the standard CSH (and many variants) have already been worked out and relevant information about its particle correlations is available. The information can then be used in deriving the solution for $P_N(E, Y)$ and the spectral correlations for the present case. (A similar connection between multiparametric Gaussian ensembles without chirality and the standard CSH has been used in the past to derive the spectral correlations for the former, although the steps remain essentially the same for the two cases but the difference in confining potential is expected to manifest in long range correlations). Alternatively, for the Ch-BE, a hierarchical set of equations for the spectral correlations is derived in [24] [see Eq. (77) therein] and can directly be applied for the multiparametric chiral Gaussian ensembles [with Y in Eq. (76) of [24] now replaced by Y in Eq. (6)].

Further insights about the spectral statistics in the multiparametric chiral case can also be gained by a comparison of Eq. (9) with its nonchiral counterpart derived in [15,17,19] [see Eq. (17) of [15] or Eq. (52) of [17]]. A significant difference in the two equations arises in the form of the contribution from the repulsion part of the drift term; contrary to the nonchiral case with repulsion arising from the terms of type $\frac{1}{e_n - e_m}$, the chiral case also contains additional terms of type $\frac{1}{e_n + e_m}$ and $\frac{(\nu+1/2)}{e_n}$ (the terms arising due to existence of equal and opposite pairs of eigenvalues as well as zero eigenvalues and their repulsions). The additional terms are, however, relatively negligible for the spectral ranges $|e| \gg 0$ and Eq. (9) can be approximately reduced to the nonchiral case. This suggests analogous statistical behavior, away from $|e| = 0$, for the two cases, which is also numerically confirmed by previous studies.

B. Fluctuation measures

The Y-based formulation of the spectral JPDF, given by Eq. (9), indicates its applicability to a wide range of chiral ensembles. It also leads to the diffusion equation for nth order spectral correlation $R_n(e_1, \ldots, e_n)$, i.e., the probability density of n positive eigenvalues irrespective of the location of other ones, defined as $R_n(e_1, \ldots, e_n) = \frac{N!}{(N-n)!} \int \prod_{j=n+1}^{N} de_j\ P_e(e_1, \ldots, e_N)$. Using the spectral density formula $\rho(e) = \sum_n \delta(e - e_n)$, R_n can also be expressed as the nth order ensemble averaged level-density correlation: $R_n(e_1, \ldots, e_n) = \langle \rho(e_1)\ \rho(e_2) \ldots \rho(e_n) \rangle$ with $\langle . \rangle$ implying the ensemble average. Thus $R_n(e_1, \ldots, e_n)$, for $n > 1$, describe the local fluctuations of the spectral density $\rho(e)$ and R_1 is its ensemble average.

The spectral density in general is system dependent. For comparison of the local fluctuations imposed on different spectral density backgrounds, it is imperative to rescale or "unfold" the levels e_j by the local mean level spacing $\Delta_{\rm loc}(e)$ at the spectral point of interest, say e. The rescaled correlations can be given as $\mathcal{R}_n(r_1, \ldots, r_n; e) = \lim N \to \infty \frac{R_n(e_1, \ldots, e_N)}{R_1(e_1) \ldots R_1(e_n)}$ with $r_n = \frac{(e_n - e)}{\Delta_{\rm loc}(e)}$ and $r = e\ \Delta_{\rm loc}(e)$. The unfolding of eigenvalues, however, also rescales the parameter Y; the rescaled complexity parameter can be given as [24] (also see Sec. 6.13 of [4], [6,21–23], and references therein)

$$\Lambda_e(Y, e) = \frac{(Y - Y_0)}{[\Delta_{\rm loc}(e)]^2}. \tag{11}$$

As clear from the above, the rescaling results in an energy dependence of the diffusion parameter.

The diffusion equation for $\mathcal{R}_n$ for the chiral Brownian ensemble is discussed in [24] and is applicable for the present case too (due to analogy of the diffusion equations for P_N for the two cases) but with Y now given by Eq. (6). As discussed in [24], Λ_e is obtained by neglecting the variations of the average level density at e [24] and is therefore applicable for the nth order local correlations within an energy range, say $e \pm n\Delta_{\rm loc}(e)$, with $\Delta_{\rm loc}(e)$ dependent on the interaction among states.

Local mean level spacing

A determination of Λ_e from Eq. (11) requires a prior knowledge of $Y - Y_0$ as well as $\Delta_{\rm loc}$. While Y is explicitly given by Eq. (6), $\Delta_{\rm loc}$ depends on the underlying eigenfunction dynamics; for the eigenfunctions with nonergodic dynamics, it can be significantly different from the mean level spacing $\Delta(e)$. This can be explained as follows: while $\Delta_{\rm loc}(e)$ corresponds to only those states at energy e which are interacting, $\Delta(e)$ refers to all states at energy e irrespective of their interaction. As the eigenfunctions localized in different parts of the basis space do not interact, $\Delta_{\rm loc}(e)$ is intuitively expected to be proportional to the average correlation or localization volume at energy e [26]. Based on the above reasoning, one possible definition can be given as follows: $\Delta_{\rm loc}(e) = \frac{1}{\langle \rho_{\rm loc} \rangle}$ where

$$\rho_{\rm loc}(e) = \sum_{n=1}^{N} \phi_n \, \delta(e - e_n) \tag{12}$$

with ϕ_n as the probability of the nth eigenfunction interacting with other eigenfunctions at energy e (and therefore occupying the same region as other eigenfunctions with energies close to e). Note $\rho_{\rm loc}(e)$ in general is different from the standard local density of states. [The latter is defined as $\rho(e, j) = \sum_n |U_{jn}|^2 \delta(e - e_n)$, thus counting the eigenstates U_n having appreciable overlap with or, equivalently, located close to the basis state j in an arbitrary basis.] Instead $\rho_{\rm loc}(e)$ refers to, in our case, the number of interacting states at energy e and, therefore, to the probability of states, with their energy e, occupying the same region in basis space. Clearly, although the spread of eigenfunctions in the basis space affects $\rho_{\rm loc}(e)$ too, contrary to $\rho(e, j)$, it does not explicitly depend on the location, i.e., basis state j. Also note that both $\rho_{\rm loc}(e)$ and $\rho(e, j)$ are clearly distinct from the global density of states $\rho(e) = \sum_{n=1}^{N} \delta(e - e_n)$ too, which counts all the eigenstates at the energy e irrespective of their basis space location as well as mutual interaction.

From Eq. (12), the determination of $\rho_{\rm loc}(e)$ requires a prior knowledge of ϕ_n, but at present this is known only for the special cases. For example, for the case in which a typical eigenfunction is delocalized in the entire Hilbert space (e.g., a GOE), the above implies $\phi_n = 1$, which gives $\langle \rho_{\rm loc}(e) \rangle = R_1(e)$ and $\Delta_{\rm loc}(e) = \Delta(e)$. [Note, a GOE has a strong level repulsion and a semicircle level density: $R_1(e) = \frac{1}{\pi}\sqrt{2N - e^2}$. The latter is almost constant for a large neighborhood of $e \sim 0$ if N is large; this in turn implies $\langle \rho_{\rm loc}(e) \rangle = R_1(e)$.] Similarly, in the case of localized dynamics, e.g., although two localized states do not typically overlap they can be localized in the same region with a small probability of $\xi^d/(2N)$ [with $\xi(e)$ as the average localization radius at energy e, d as the system dimension, and $2N$ as the number of basis states] [26]. This implies $\phi_n \sim \frac{\xi^d}{2N}$, which gives $\rho_{\rm loc}(e) = \frac{\xi^d}{2N} R_1(e)$. Using $R_1(e) = \frac{1}{\Delta(e)}$, this leads to

$$\Delta_{\rm loc}(e) = \Delta(e) \, \frac{2N}{\xi^d} \tag{13}$$

(with $\xi^d/2N$ as the probability of eigenfunctions localized in the same region of basis space). For cases where the eigenfunctions are exponentially localized, e.g., in the standard Anderson Hamiltonian (a single particle moving in a random potential), $\xi^d(e)$ can be approximated by the average inverse participation ratio $\langle I_2(e) \rangle$ of the eigenfunctions with energies $\sim e$: $\xi^d \approx (\langle I_2 \rangle)^{-1}$. [For an eigenfunction U_n described in a N-dimensional basis, I_2 is defined as $I_2(U_n) = \sum_{k=1}^{N} |U_{kn}|^4$. Following from the definition, $I_2(U_n) \propto 1/N$ for U_n extended throughout basis space, and $I_2(U_n) = 1$ for U_n localized on just one basis state. In general, I_2 varies with energy e and it is a standard practice to consider an averaged I_2 of all eigenfunctions within a given spectral range in which the average spectral density varies smoothly.] Note, however, that the $\xi - I_2$ relation mentioned above is not valid in general and one has to use alternate routes to determine ξ.

As discussed in [24], Λ_e is the only parameter (besides the energy range of interest) which appears in the differential equations determining the local spectral fluctuations. The latter are therefore expected to be analogous for two different ensembles if (i) both have the same Λ_e value and (ii) both evolve from an analogous initial condition (statistically). [Note, as mentioned below Eq. (7), that the final end point of the diffusion is a chiral GOE or GUE with the matrix element variance dependent on γ.] Equivalently, the ensembles with different system conditions but subjected to the same global constraints (e.g., Hermitian as well as chiral nature of the H matrix in the present paper) statistically correspond to different crossover points on a specific curve (based on the global constraints) lying between the initial point Y_0 and the end point Ch-GOE or Ch-GUE.

IV. NUMERICAL VERIFICATION OF SINGLE PARAMETRIC FORMULATION

To verify the above prediction, we numerically compare the spectral fluctuations of four multiparametric Gaussian ensembles of real-symmetric matrices as well as complex Hermitian chiral matrices with different variance types. The ensemble details needed to determine $Y - Y_0$ as well as Δ_e and thereby Λ_e are discussed below. The section also illustrates how different ensembles, if subjected to the same matrix constraints, can be justified to evolve from the same initial condition.

A. Details of the ensembles

The ensembles can briefly be described as follows.

1. Chiral Anderson ensemble

Within the tight-binding approximation, the Hamiltonian H of a d-dimensional bipartite lattice with $\mathcal{N}_a$ unit cells, each consisting of two atoms, with a single orbital contributing for each atom, can be given as

$$H = \sum_{x,y} V_{xy} \, c_x^\dagger c_y \tag{14}$$

with $c_x^\dagger$ and c_x as the particle creation and annihilation operators on the site x, V_{xx} as the on-site energy, and V_{xy} as the hopping between sites x and y. Here $x = (m, \alpha)$ with m as the label for the d-dimensional unit cell and α as the atomic label, where $\alpha = a, b$. The motivation for choice of this system

comes from the rich physical properties it has been shown to display by previous studies [27].

To preserve chiral symmetry, here we consider the case with zero diagonal disorder [13], a Gaussian hopping between atoms within the same unit cell, and an isotropic Gaussian hopping between z nearest neighbor sites on different unit cells; this implies (i) $V_{xx} = 0$, (ii) $V_{xy} \neq 0$ and is Gaussian distributed for $x = (m, a), y = (m, b)$, (iii) $V_{xy} \neq 0$ and is Gaussian distributed if $x = (m, \alpha)$ and $y = (m-1, \beta)$ or $(m+1, \beta)$ with $\beta = a, b$ but $\beta \neq \alpha$, and (iv) $V_{xy} = 0$ for all other x, y pairs. Henceforth this case is referred as Ch-AE.

In site basis, the condition (i) results in a chiral structure of matrix H in Eq. (1) The conditions (ii) and (iii) lead to nonzero C_{kk} and C_{kl}, respectively, for k, l pairs corresponding to z nearest neighbor sites on different unit cells. The ensemble density in this case is given by (3) with

$$h_{kk} = \langle C_{kk}^2 \rangle = w^2/12, \quad h_{kl} = \langle C_{kl}^2 \rangle = f_1\ w_s^2/12,$$
$$b_{kl} = \langle C_{kl} \rangle = f_2\ t \tag{15}$$

where $f_1(kl) = 1, f_2(k, l) = 1$ for $\{k, l\}$ pairs representing hopping, and $f_1(k, l), f_2(k, l) \to 0$ for all $\{k, l\}$ values corresponding to disconnected sites. From Eq. (6), the ensemble complexity parameter in this case is [16]

$$Y = -\frac{\beta N}{2M\gamma} \ln\left[|1 - \gamma w^2/6||1 - \gamma w_s^2/6|^z\ |t + \delta_{t0}|^{2z}\right] + c_0 \tag{16}$$

where $M = \beta N(N + 2z)$ with $2\beta z N$ as the number of nearest neighbors which depends on the lattice conditions as well as the dimensionality d of the system. Here c_0 is a constant of integration (determined by the initial condition on the ensemble).

To determine Y_0, the initial state is chosen as a clean bipartite lattice with sufficiently far off atoms resulting in zero hopping (i.e., both $w = w_s = 0$); consequently the initial ensemble corresponds to a localized eigenfunction dynamics with Poisson spectral statistics (with chiral constraint) and $Y_0 = c_0$. Substitution of Eq. (16) in Eq. (11) with $\Delta_{\rm loc}(e) = \frac{2N\langle I_2 \rangle}{R_1}$ and $\overline{\langle I_2 \rangle}$ as the typical ensemble as well as spectral averaged inverse participation ratio at e leads to the spectral complexity parameter:

$$\Lambda_{e,A}(Y, N, e) = \frac{-R_1^2}{8\gamma N^3\ \overline{\langle I_2 \rangle}^2}\ \ln[|1 - \gamma\ w^2/6||1 - \gamma\ w_s^2/6|^z \times |t + \delta_{t0}|^{2z}]. \tag{17}$$

2. Chiral Rosenzweig-Porter ensemble

This is a chiral variant of the standard Rosenzweig-Porter ensemble [21,28], with $\rho(H)$ given by Eq. (4) where

$$h_{kk;s} = \langle C_{kk;s}^2 \rangle = 1, \quad h_{kl;s} = \langle C_{kl;s}^2 \rangle = \frac{1}{(1+\mu)}, \qquad k \neq l,$$
$$b_{kl;s} = \langle C_{kl;s} \rangle = 0 \quad (\forall\ k, l) \tag{18}$$

with $0 < \mu < \infty$; the limits $\mu = 0$ and ∞ correspond to a Ch-GOE and a matrix ensemble with diagonal chiral blocks, respectively. Henceforth this case is referred as Ch-RPE. Substitution of the above values in Eq. (6) gives Y for this case:

$$Y = -\frac{\beta N(N-1)}{2M\gamma} \ln\left[1 - \frac{2\gamma}{(1+\mu)}\right] + c_0 \tag{19}$$

with $M = \beta N(N + \nu) = \beta N^2$ (with $\nu = 0$ in our numerics) and c_0 as a constant of integration (determined by the initial condition on the ensemble).

Choosing the initial condition with $\mu \to \infty$ corresponds to an ensemble of H matrices, with its chiral blocks as diagonal C matrices and the spectral statistics as Poisson statistics (with chiral constraint). From Eq. (19), this implies $Y_0 = c_0$ and $Y - Y_0 \approx \frac{1}{\mu}$ (for $\mu \gg 1$). This on substitution in Eq. (11) leads to the spectral complexity parameter for the Ch-RPE case:

$$\Lambda_{e,B}(e) = \frac{Y - Y_0}{\Delta_{\rm loc}(e)^2} \approx \frac{R_1^2}{\mu}. \tag{20}$$

Here the second equality is obtained by using $\Delta_{\rm loc}(e) = \Delta(e) = \frac{1}{R_1(e)}$. As clear from the above, $\Lambda_{e,B}$ depends on three parameters, namely, μ, matrix size N, as well as the spectral location e chosen for the analysis of the local fluctuations.

The ensemble density with distribution parameters given by Eq. (18) is analogous to a specific class of Ch-BE [24], namely, that arising due to a single parametric perturbation of a chiral ensemble, with Poisson statistics for nonzero eigenvalues, by a Ch-GOE ensemble; we henceforth refer to the Ch-RPE case as the Ch-BE case.

3. Chiral Gaussian ensemble with power law decay

The C-matrix ensemble in this case consists of independently distributed Gaussian entries with zero mean and a power law decay of variances away from the diagonal. The ensemble density $\rho(H)$ can again be described by Eq. (4) with

$$h_{kl} = \langle C_{k,l}^2 \rangle = \frac{1}{1 + \frac{|k-l|^2}{b^2}}, \qquad b_{kl} = \langle C_{kl} \rangle = 0 \quad \forall\ k, l \tag{21}$$

where b is an arbitrary parameter (the corresponding nonchiral variant was first discussed in detail in [29] and later in many works, e.g., [15,16,20,26]).

Substitution of Eq. (21) in Eq. (6) gives

$$Y = -\frac{\beta}{2M\gamma}\left[\sum_{r=0}^{N} g_r\ (N - r)\ \ln\left(1 - \frac{2\gamma}{1 + (r/b)^2}\right)\right] + c_0 \tag{22}$$

with the number of independent elements $M = \beta N^2$, $r \equiv |k - l|$, and $g_r = (2 - \delta_{r0})$. Here the case $b \ll 1$ corresponds to the H ensemble with diagonal C matrices with Poisson spectral statistics and can therefore be chosen as the initial ensemble. The choice leads to $Y_0 = -\frac{N\beta}{2M\gamma} \ln(1 - 2\gamma) + c_0 \approx c_0$ (for large N).

TABLE I. Ensemble and spectral parameters used for Λ_e in Fig. 3 for Ch-AE. Here the first column lists the approximate Λ_e values, referred to as Λ in different parts of Fig. 3. The columns 2–4 list the ensemble parameters, i.e., matrix size, ensemble size, and squared disorder strength w^2 used in Eqs. (15) and (17) with fixed $w_s^2 = 12$ and $t = 0$. The columns 5–7 list the spectral parameters, namely, energy e, ensemble averaged level density $F(e) = R_1(e)/2N$, and inverse participation ratio at e used in Eq. (17) with resulting Λ_e values given in column 8 as $\Lambda_{\rm calc}$. Here $\gamma = 1/4$ is fixed for all cases. We also compare the numerical results for $P(r)$ for each Λ value with Eq. (29) with $\alpha(\beta_t) = \Lambda - 1.69\,(1-\beta_t) + 0.89\,(1-\beta_t)^5$. The columns 9 and 10 list the values of fitted parameters β_t and C_t.

Λ	N	Ensemble size	w^2	$-e$	$F(e)$	$\langle I_2(e)\rangle$	$\Lambda_{\rm calc}$	β_t	C_t
	512	5000	12	1.39	0.143	0.02	0.69		
0.7	1058	2500	12	1.11	0.147	0.014	0.72	0.88	3.6
	512	5000	36	0.04	0.2295	0.032	0.696		
	1058	2500	36	0.04	0.233	0.0224	0.71		
	512	5000	12	1.84	0.135	0.025	0.39		
0.38	1058	2500	12	1.58	0.137	0.018	0.379	0.88	4.07
	512	5000	36	0.425	0.14	0.026	0.39		
	1058	2500	36	0.095	0.16	0.021	0.38		
	512	5000	12	2.2	0.124	0.0326	0.196		
0.2	1058	2500	12	1.91	0.13	0.023	0.209	0.8	4.216
	512	5000	36	1.45	0.1205	0.0312	0.202		
	1058	2500	36	0.71	0.131	0.0237	0.2		
	512	5000	12	2.65	0.109	0.0486	0.068		
0.07	1058	2500	12	2.39	0.116	0.035	0.072	0.66	3.7
	512	5000	36	2.42	0.103	0.045	0.071		
	1058	2500	36	1.96	0.114	0.034	0.073		

The above along with Eq. (11), with $\Delta_{\rm loc}(e) = \frac{2N\langle I_2\rangle}{R_1}$, then leads to

$$\Lambda_{e,P}(b,e) = \frac{-R_1^2}{8\gamma N^4\,\overline{\langle I_2\rangle}^2}\left[\sum_{r=1}^{N}(N-r)\ln\left(1-\frac{2\gamma}{1+(r/b)^2}\right)^2\right]. \tag{23}$$

The spectral statistics of a chiral Gaussian ensemble with power law decay (Ch-PE) therefore shows a crossover from Poisson (for $\Lambda_{e,P} \to 0$ as $b \to 0$) to chiral GOE behavior (for $\Lambda_{e,P} \to \infty$ as $b \to \infty$).

4. Chiral Gaussian ensemble with exponential decay

Here the ensemble of C matrices corresponds to an exponential decay of the variances away from the diagonals C_{kk} but with mean $\langle C_{kl}\rangle = 0$ for all k, l. The $\rho(H)$ is again given by Eq. (4) with

$$h_{kl} = \langle C_{kl}^2\rangle = \exp\left(-\frac{|k-l|}{b}\right)^2, \quad b_{kl} = \langle C_{kl}\rangle = 0 \quad \forall\ k,l \tag{24}$$

with b as an arbitrary parameter [the nonchiral variant of Eq. (24) is discussed in many studies, e.g., [15,16,20,26]]. Henceforth this case is referred as Ch-EE.

Equation (6) now gives

$$Y = -\frac{\beta}{2M\gamma}\left[\sum_{r=0}^{N} g_r\,(N-r)\ln\left(1-\frac{2\gamma}{\exp(\frac{r}{b})^2}\right)\right] + c_0 \tag{25}$$

with $M = \beta N^2$, $r \equiv |k-l|$, and $g_r = 2 - \delta_{r0}$.

To keep analogy with the other ensembles described above, here again the initial ensemble for C is chosen to be that of the diagonal matrices with a Poisson spectral statistics which corresponds to $Y_0 = -\frac{N\beta}{2M\gamma}\ln(1-2\gamma) + c_0 \approx c_0$ (for large N). Referring to the localization length as ξ and using $\Delta_{\rm loc}(e) = \frac{2N}{\xi}\,\Delta(e)$, the spectral complexity parameter now becomes

$$\Lambda_{e,E}(b,e) = \frac{-\xi^2 R_1^2}{8\gamma N^4}\left[\sum_{r=1}^{N}(N-r)\ln\left(1-\frac{2\gamma}{\exp(\frac{r}{b})^2}\right)\right]. \tag{26}$$

B. Numerical analysis

For numerical analysis of local spectral fluctuations for each case mentioned in Sec. IV A, we exactly diagonalize (using LAPACK, a standard software library for numerical linear algebra subroutines for complex matrices [30]) the ensembles for many system parameters but with a fixed $\gamma = 1/4$. The C matrix chosen for all cases considered here is a $N \times N$ square matrix which corresponds to $\nu = 0$. The other system-related details used in our numerics for each case are as follows (also given in Tables I–V).

(i) For the case of Ch-AEs, we consider the ensembles of $2N \times 2N$ matrix H [Eq. (14)] for a two-dimensional ($d = 2$) bipartite square lattice (of linear size L with $L^2 = 2N$) subjected to periodic boundary conditions; the ensemble parameters are given by Eq. (15) with $z = 4$. Variation of matrix size and disorder strength leads to four different ensembles: one consisting of 5000 matrices of size $2N = 1024$ and another consisting of 2500 matrices of size $2N = 2116$, each analyzed for two disorder strengths $w^2 = 12$ and 36 (keeping $w_s^2 = 12$ and $t = 0$ for both cases).

TABLE II. Ensemble and spectral parameters used for Λ_e in Fig. 4 for Ch-BE. The details here are the same as in Table I, except now the ensemble and spectral parameters refer to Eqs. (18) and (20). Here again $\gamma = 1/4$ is fixed for all cases. Note: In this case, $\langle I_2 \rangle$ is not required for Λ_e calculation.

Λ	N	Ensemble size	c	$-e$	$F(e)$	Λ_{calc}	β_t	C_t
	500	5000	1	0.08	0.2856	0.326		
0.33	864	2890	1	0.09	0.2846	0.324	1	4.7
	500	5000	0.4	1.35	0.179	0.32		
	864	2890	0.4	1.345	0.181	0.327		
	500	5000	1	1.19	0.195	0.152		
0.15	864	2890	1	1.22	0.195	0.152	0.93	4.82
	500	5000	0.4	1.87	0.122	0.148		
	864	2890	0.4	1.82	0.122	0.148		
	500	5000	1	1.65	0.143	0.081		
0.08	864	2890	1	1.66	0.142	0.08	0.83	4.52
	500	5000	0.4	2.14	0.0897	0.08		
	864	2890	0.4	2.14	0.09	0.081		
	500	5000	1	2.3	0.073	0.021		
0.02	864	2890	1	2.34	0.072	0.02	0.6	3.3
	500	5000	0.4	2.75	0.045	0.02		
	864	2890	0.4	2.72	0.045	0.02		

(ii) For the case of Ch-RPEs, we choose the ensemble described by Eq. (18) with $\mu = c\,N^2$ [the choice is motivated by previous studies of nonchiral Rosenzweig-Porter ensembles (or Brownian ensembles) which confirm this μ value as a critical point of the statistics [16,21]]. The ensemble is exactly diagonalized for two different c values, i.e., $c = 1$ and 0.4, each case considered for two different ensembles: one consisting of 5000 matrices of sizes $2N = 1000$ and another consisting of 2890 matrices of size $2N = 1728$.

(iii) For the case of Ch-PEs, the numerics is considered for the ensemble (21) of 5000 matrices of size $2N = 1000$ and another of 2500 matrices of size $2N = 2000$; each ensemble is analyzed for two b values, i.e., $b = 0.5$ and 0.75.

(iv) For the case of chiral Gaussian ensembles with exponential decay (Ch-EEs), here again we consider an ensemble (24) of 5000 matrices of size $2N = 1000$ and another of 2500 of size $2N = 2000$; both ensembles are analyzed for two b values, i.e., $b^2 = 100$ and 144.

The local fluctuations of the spectral density of a complex system are often imposed on a smooth background, i.e., average spectral density, varying from one system to another. It is necessary, for a meaningful comparison of the statistics, to rescale the spectrum by the ensemble averaged level density $R_1(e)$ (referred to as unfolding) [4]. Due to frequent unavailability of the analytical form of $R_1(e)$ for complex systems, the standard route is to determine it through numerical calculation, but for systems, the $R_1(e)$ of which is not a smooth function of energy the unfolding procedure becomes nontrivial even if $R_1(e)$ is analytically known and the spectrum is stationary. Further, in the case of nonstationary spectrums, there are additional complications; this is because the fluctuations remain energy dependent even after unfolding [as

TABLE III. Ensemble and spectral parameters used in Fig. 5 for Ch-PE. The details here are the same as in Table I, except now the ensemble and spectral parameters refer to Eqs. (21) and (23).

Λ	N	Ensemble size	b	$-e$	$F(e)$	$\langle I_2(e) \rangle$	Λ_{calc}	β_t	C_t
	500	5000	0.5	1.53	0.1807	0.0184	0.1405		
0.14	1000	2500	0.5	1.55	0.177	0.0125	0.146	1	5.32
	500	5000	0.75	2.29	0.123	0.0179	0.138		
	1000	2500	0.75	2.3	0.118	0.01195	0.143		
	500	5000	0.5	1.69	0.164	0.0228	0.075		
0.07	1000	2500	0.5	1.72	0.162	0.0163	0.072	1	5.434
	500	5000	0.75	2.42	0.108	0.022	0.0706		
	1000	2500	0.75	2.46	0.10857	0.0159	0.068		
	500	5000	0.5	1.833	0.148	0.0287	0.038		
0.037	1000	2500	0.5	1.85	0.147	0.02054	0.037	1	5.43
	500	5000	0.75	2.55	0.098	0.0276	0.036		
	1000	2500	0.75	2.54	0.0968	0.0191	0.037		
	500	5000	0.5	2.04	0.1169	0.0433	0.0106		
0.01	1000	2500	0.5	2.04	0.1217	0.0319	0.0106	0.95	5.09
	500	5000	0.75	2.75	0.0785	0.0429	0.0098		
	1000	2500	0.75	2.7	0.08	0.0287	0.011		

TABLE IV. Ensemble and spectral parameters used in Fig. 6 for Ch-EE. The details here are the same as in Table II, except now the ensemble and spectral parameters refer to Eqs. (24) and (26). Note here again, $\langle I_2 \rangle$ is not needed for Λ_e calculation.

Λ	N	Ensemble size	b^2	$-e$	$F(e)$	Λ_{calc}	β_t	C_t
	500	5000	100	0.116	0.085	0.297		
0.3	1000	2500	100	0.11	0.084	0.29	0.856	4.17
	500	5000	144	0.12	0.0774	0.298		
	1000	2500	144	0.127	0.0765	0.29		
	500	5000	100	2.14	0.0734	0.221		
0.22	1000	2500	100	1.995	0.0734	0.222	0.836	4.16
	500	5000	144	2.07	0.0674	0.225		
	1000	2500	144	2.36	0.0667	0.222		
	500	5000	100	4.86	0.0604	0.15		
0.15	1000	2500	100	4.93	0.061	0.153	0.733	3.87
	500	5000	144	5.29	0.0555	0.153		
	1000	2500	144	5.41	0.0549	0.1508		
	500	5000	100	7.93	0.0216	0.019		
0.02	1000	2500	100	7.98	0.024	0.023	0.335	2.13
	500	5000	144	8.75	0.01985	0.0196		
	1000	2500	144	8.66	0.0206	0.21		

indicated by the energy dependence of $\Lambda_e(e)$] [16,17,24]. For comparison of local statistics, therefore, ideally one should consider an ensemble averaged fluctuation measure at a specific energy point, say e, without any spectral averaging. This in general requires consideration of huge ensembles and runs into practical technical issues. Fortunately, in the spectral regions where Δ_{loc} varies very slowly, it is possible to choose an optimized range in the neighborhood of e, sufficiently large for good statistics but keeping a mixing of different statistics at minimum. This is, however, not the case for the regions with sharp change of Δ_{loc}; the latter leads to a rapidly changing Λ_e and it is numerically difficult to consider a spectral range with an appropriate number of levels without mixing of different statistics. This compels us to consider, for numerical analysis, only 1% of the total eigenvalues taken from a range $\Delta_{\text{loc}}(e)$ around e if e is in the bulk. A rapid variation of the spectral density (e.g., near $e = 0$ or the spectral edge) however permits one to consider a very small spectral range (0.5–1%); this in turn gives rise to errors in Λ_e calculations (as evident from Figs. 7 and 8).

Almost all standard spectral fluctuation measures, e.g., nearest neighbor spacing distribution and number variance, are sensitive to unfolding issues which cannot be ignored especially in the case of a nonstationary spectrum. This motivated the study [31] to introduce a new measure, namely, the nearest neighbor spacing ratio distribution $P(r) = \sum_{i=1}^{N-1} \langle \delta(r - r_i) \rangle$ with r defined as the ratio of consecutive spacings between nearest neighbor levels: $r_i = s_{i+1}/s_i$ where $s_i = e_{i+1} - e_i$ is the distance between two nearest neighbor eigenvalues [31,32]. As the ratio r does not depend on the

TABLE V. Ensemble and spectral parameters used in Fig. 7 for intersystem analogy for the $\beta = 1$ case. The details here are the same as in Table I, except now the parameter given in column 4 refers to the ensemble mentioned in column 2 [given by Eqs. (15), (18), (21), and (24)]. Similarly the spectral parameters given in columns 5–7 are used for Λ_e calculation of the systems in column 2 [with their Λ_e given by Eqs. (17), (20), (23), and (26)]. Here the ensemble size is kept fixed (with 5000 matrices) for all cases.

Λ	System	N	Disorder parameter	$-e$	$F(e)$	$\langle I_2(e) \rangle$	Λ_{calc}	β_t	C_t
	Ch-AE	512	$w^2 = 12$	2	0.128	0.0281	0.28		
0.28	Ch-BE	500	$c = 0.4$	1.41	0.167		0.278	0.94	4.53
	Ch-PE	500	$b = 0.5$	1.27	0.202	0.0145	0.282		
	Ch-EE	500	$b^2 = 100$	0.116	0.084		0.0289		
	Ch-AE	512	$w^2 = 12$	2.2	0.124	0.0326	0.196		
0.2	Ch-BE	500	$c = 0.4$	1.65	0.142		0.2	0.92	4.62
	Ch-PE	500	$b = 0.5$	1.41	0.191	0.0163	0.2		
	Ch-EE	500	$b^2 = 100$	2.78	0.0715		0.209		
	Ch-AE	512	$w^2 = 12$	2.36	0.1206	0.037	0.143		
0.14	Ch-BE	500	$c = 0.4$	1.87	0.12		0.144	0.87	4.46
	Ch-PE	500	$b = 0.5$	1.53	0.1807	0.0184	0.1405		
	Ch-EE	500	$b^2 = 100$	5.09	0.0582		0.139		
	Ch-AE	512	$w^2 = 12$	2.59	0.113	0.0457	0.082		
0.08	Ch-BE	500	$c = 0.4$	2.14	0.0897		0.08	0.78	4.18
	Ch-PE	500	$b = 0.75$	2.39	0.112	0.021	0.083		
	Ch-EE	500	$b^2 = 100$	6.6	0.045		0.083		

TABLE VI. Ensemble and spectral parameters used in Fig. 8 for intersystem analogy for the $\beta = 2$ case. The other details here are the same as given in the caption of Table V.

Λ	System	N	Disorder parameter	$-e$	$F(e)$	$\langle I_2(e)\rangle$	$\Lambda_{\rm calc}$	β_t	C_t
	Ch-AE	512	$w^2 = 84$	4.36	0.0693	0.017	0.12		
0.12	Ch-BE	500	c = 0.4	2.7	0.111		0.123	1.89	22.445
	Ch-PE	500	b = 0.3	1.67	0.1938	0.01316	0.121		
	Ch-EE	500	$b^2 = 144$	1.04	0.04917		0.12		
	Ch-AE	512	$w^2 = 84$	1.33	0.0693	0.0204	0.083		
0.08	Ch-BE	500	c = 0.4	2.91	0.09		0.081	1.745	21.18
	Ch-PE	500	b = 0.3	1.83	0.1841	0.01548	0.0795		
	Ch-EE	500	$b^2 = 144$	7.26	0.0404		0.081		
	Ch-AE	512	$w^2 = 84$	0.98	0.06585	0.025	0.05		
0.05	Ch-BE	500	c = 0.4	3.08	0.072		0.051	1.6	19.145
	Ch-PE	500	b = 0.3	1.96	0.1744	0.0183	0.051		
	Ch-EE	500	$b^2 = 144$	9.76	0.0318		0.05		
	Ch-AE	512	$w^2 = 84$	5.63	0.0606	0.0349	0.02		
0.02	Ch-BE	500	c = 0.4	3.46	0.053		0.028	1.26	13.7
	Ch-PE	500	b = 0.3	2.14	0.155	0.0248	0.021		
	Ch-EE	500	$b^2 = 144$	11.8	0.0202		0.02		

local density of states, an unfolding of the spectrum for $P(r)$ is not required [31]. Further, $P(r)$ being a short range fluctuation measure, it reduces the chances of mixing spectral statistics. For the spectral statistics in the Poisson and Wigner-Dyson limit, $P(r)$ can be given as [32]

$$P(r) = \frac{c_\beta\ (r + r^2)^\beta}{(1 + r + r^2)^{1+(3/2)\beta}} \qquad \text{Wigner-Dyson} \qquad (27)$$

$$= \frac{1}{(1 + r)^2} \qquad \text{Poisson} \qquad (28)$$

with $c_1 = \frac{27}{8}$ and $c_2 = \frac{81\sqrt{3}}{4\pi}$.

In the regime intermediate to Poisson and GOE or GUE, our theory suggests $P(r)$ to be governed only by Λ_e. A recent study [33] has indeed postulated a one-parameter distribution for $P(r)$ in the intermediate regime:

$$P(r; \beta_t, \gamma(\beta_t)) = C_{\beta_t}\ \frac{(r + r^2)^{\beta_t}}{[(1 + r)^2 - \alpha(\beta_t)\ r]^{1+1.5\beta_t}} \qquad (29)$$

with C_{β_t} as a normalization constant defined by the condition $\int_0^\infty dr\ P(r) = 1$. Here $\alpha(\beta_t)$ is defined by the ideas based on information entropy [33]: with $\alpha(\beta_t) = 0.92$–$1.42\ (2 - \beta_t) + 0.01\ (2 - \beta_t)^7$ (for $\beta = 2$) and $\alpha(\beta_t) = 0.80$–$1.69\ (1 - \beta_t) + 0.89\ (1 - \beta_t)^5$ (for $\beta = 1$) with β_t as the fitting parameter: $0 \leqslant \beta_t \leqslant \beta$. The desire to understand the connection between our Λ_e and α in Eq. (29) led us to fit our numerical results for $P(r)$ with Eq. (29); our analysis suggests a linear relation between them (see Tables I–VI).

From Eq. (11), Λ_e for an ensemble can be determined if $R_1(e)$ as well as ensemble averaged localization length ξ are known. The latter can often be estimated (e.g., for Ch-AEs and Ch-PEs) from the average inverse participation ratio $\langle I_2\rangle$. The theoretical formulations for $R_1(e)$ and $\langle I_2\rangle$ for the cases used in our numerics are, however, not known. (It is worth emphasizing here that such information is in general not available for most of the multiparametric ensembles, especially those with sparse matrix structures.) However, for the nonchiral BE case, with $\mu = cN^2$, $R_1(e)$ is theoretically known to be a Gaussian [34] but its validity for Ch-BE is not *a priori* obvious. Further, while the average level density of the chiral Anderson Hamiltonian is discussed in previous studies (see, for example, [13] and references therein), it is not exact and also based on the numerical analysis for specific system parameters. In the absence of a theoretical formulation, the option left to us is to determine $R_1(e)$ and ξ by a numerical analysis. For the Ch-EE-case, however, we find that the approximation $\xi \sim \langle I_2\rangle^{-1}$ does not seem to be valid; instead using $\xi \approx \sqrt{2N}$ (following insight based on numerics) gives results consistent with our theoretical claim about Λ_e.

Figure 1 illustrates the energy as well as system dependence of the scaled level density $F(e) = R_1(e)/2N$ for the ensembles (i)–(iv). As clear from Figs. 1(a), 1(c) and 1(d), Ch-AE, Ch-PE, and Ch-EE show a strong dependence of $F(e)$ on the variances h_{kl} of the matrix elements C_{kl} but insensitivity to the matrix size N. In contrast, Fig. 1(b) for Ch-BE indicates the independence of $F(e)$ from both h_{kl} as well as N. An important point worth noting here is a weakly singular level density near $e = 0$ in Fig. 1(a) (although $\nu = 0$ for our case); the behavior arises due to choice of zero mean off-diagonal randomness in the C matrix (for its nonzero elements) and is consistent with previous studies [13]. A weaker singularity displayed in Figs. 1(c) and 1(d) is a result of weaker relative sparsity of the C matrix elements in the case of Ch-PE and Ch-EE. The absence of singularity in Fig. 1(b) results from the lack of sparsity in the C matrix of Ch-BE; note the Gaussian form in Fig. 1(b) is consistent with theoretical prediction of [34] (although the latter study is on nonchiral BEs).

Figure 2 illustrates the energy as well as system dependence $\langle I_2\rangle$ for the four ensembles. As Figs. 2(a) and 2(c) indicate, $\langle I_2\rangle$ for Ch-AE and Ch-PE is sensitive to the variance of the matrix elements but not to the matrix sizes N. Although $\langle I_2\rangle$ does not appear in our Λ_e formulation for Ch-BE and Ch-EE, its behavior for these cases is still displayed in Figs. 2(b) and 2(d) for comparison with other cases.

Using $F(e)$ and $\langle I_2\rangle$ (the latter used only for Ch-AE and Ch-PE) at a given e from Figs. 1 and 2, we calculate $\Lambda_e(e)$ for the four ensembles. As Eqs. (20), (17), (23), and (26) indicate,

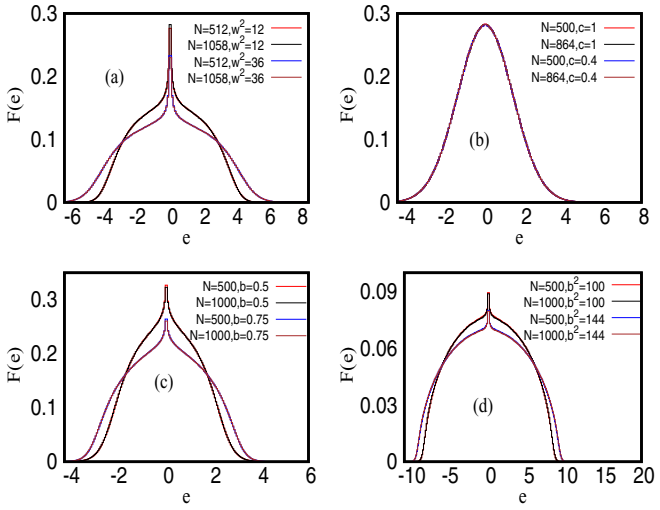

FIG. 1. Density of states. The determination of spectral complexity parameter Λ_e requires a prior knowledge of the ensemble averaged level density. The parts (a), (b), (c), (d) display the scaled level density $F(e) = R_1(e)/2N$ for the cases Ch-AE, Ch-BE, Ch-PE, and Ch-EE, respectively. As mentioned in the main text, C chosen for our numerics is an $N \times N$ square matrix, thus implying $\nu = 0$; note that, however, does not imply that the level density will dip near $e = 0$. As clear from the parts (a), (c), and (d), Ch-AE, Ch-PE, and Ch-EE show a strong dependence of $F(e)$ on the variances h_{kl} of the matrix elements but insensitivity to the matrix size N. In contrast, part (b) for Ch-BE indicates an independence of $F(e)$ from h_{kl} as well as N.

Λ_e for each ensemble not only depends on the energy range e of interest but also on at least two other system parameters. The analogy of the local spectral statistics among the ensembles can then manifest in many ways. More clearly, if indeed governed only by Λ_e as predicted by our theory, an

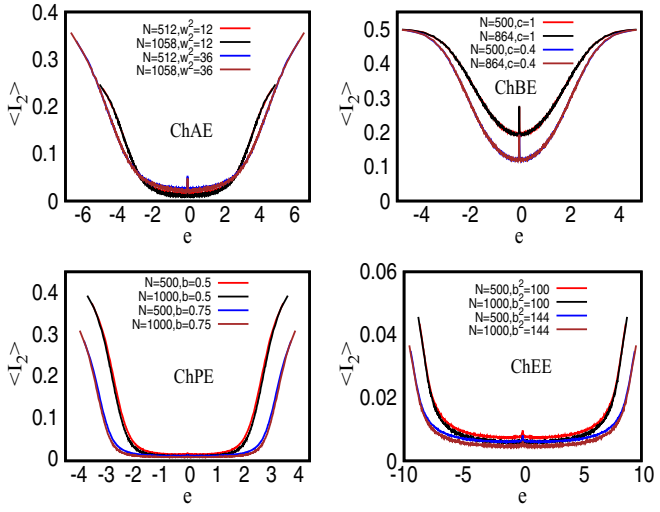

FIG. 2. Ensemble averaged inverse participation ratio. As mentioned in the text, a prior knowledge of $\langle I_2 \rangle$ is needed to determine Λ_e for some cases; the figure illustrates the e-dependence of IPR for Ch-AE, Ch-RPE, Ch-PE and Ch-EE. As clear from each part, $\langle I_2 \rangle(e)$ behavior is sensitive to the variance of the matrix elements.

analogy for the local correlations at different energies can occur within the same ensemble but by varying other distribution parameters. For example, if $\Lambda_{e,x}(e_1, s_1) = \Lambda_{e,x}(e_2, s_2)$ with s_1 and s_2 referring to two different sets of system parameters for a specific ensemble "x" (e.g., $x = A, B, P, E$), the local correlations of the latter at e_1, s_1 are expected to be analogous to those at e_2, s_2; below, this is referred to as the "intrasystem" analogy. Similarly if Λ_e for different ensembles are equal (for same or different e values), their local correlations should be analogous too. For example, if $\Lambda_{e,x}(e_1) = \Lambda_{e,y}(e_2)$ with $x, y = A, B, P, E$, the local correlations for the ensemble x at e_1 are then predicted to be analogous to that of y at e_2 (referred to below as the "intersystem" analogy).

An important point to note here is the following: for $\Lambda \to 0, \infty$ (stationary limits), $P(r)$ is expected to approach Poisson and GOE or GUE limits, respectively, for almost all e ranges and becomes e independent. A variation of the statistics from Poisson to GOE or GUE limits, as e varies, occurs only for finite nonzero $\Lambda_e(e)$ (the latter corresponds to a critical regime of the statistics for finite N and a critical point in large N limits). The condition $\Lambda_{e,x}(e_1, s_1) = \Lambda_{e,x}(e_2, s_2)$ can therefore be satisfied only if Λ_e remains finite, nonzero, as well as e dependent for both cases.

To confirm our theoretical prediction, here we numerically verify both these analogies by comparing $P(r)$ for a number of combinations. The details are as follows.

1. Intrasystem analogy

Here we are concerned with the local spectral statistics of the ensembles consisting of the same Hamiltonian matrix representing a system, say x. The ensemble parameters for the analogs can then be obtained by invoking the following condition:

$$\Lambda_{e,x}(e_1, s_1) = \Lambda_{e,x}(e_2, s_2) = \Lambda_{e,x}(e_3, s_3) = \Lambda_{e,x}(e_4, s_4) \tag{30}$$

with $\Lambda_{e,x}$ given by Eqs. (17), (20), (23), and (26) for $x = A, B, P, E$, respectively. As mentioned above, the ensembles chosen should be nonstationary. The above analogy being sensitive to error in Λ calculation, we avoid mixing of the statistics by taking only 1% of the eigenvalues from the chosen energy range if $|e| > 0$; the percentage of levels considered for $e \sim 0$, however, is less (between 0.5 and 1%).

For comparisons of the ensembles in different energy regimes, it is preferable to choose the same number of levels for each case. For this purpose, the number of matrices M in the ensemble for each matrix size N is chosen so as to give approximately 2.5×10^4 eigenvalues for the analysis. Further as Eqs. (16), (19), (22), and (25) indicate, Y is β independent. Thus Λ_e depends on β only through $\Delta_{\rm loc}$ (more specifically through average localization length ξ). The effect, however, is quantitative only and does not lead to any qualitatively new insights in the case of intrasystem analogy. To avoid repetition, here we consider the $\beta = 1$ case only.

Figure 3 displays a comparison of $P(r)$ behavior for Ch-AE obtained from four different combinations of disorder w and system size N at a specific energy e. Here the parametric combinations are chosen such that Eq. (30) is satisfied (with $\gamma = 1/4$). (The numerical procedure used for the purpose is

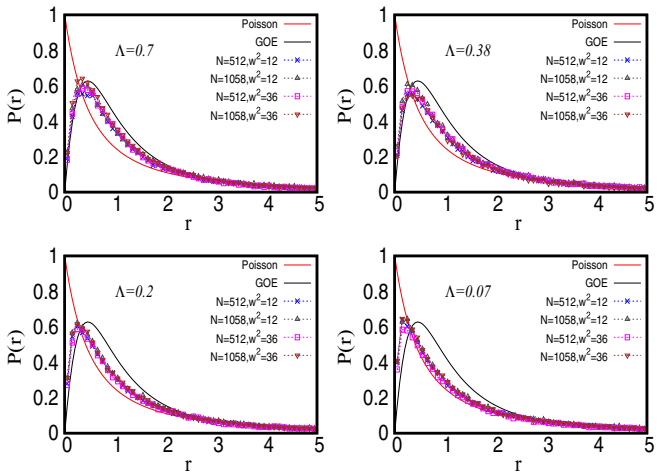

FIG. 3. Intrasystem analogy: nearest neighbor spacing ratio distribution for Ch-AE. As Λ_e for Ch-AE depends on many system parameters, e.g., w, w_s, t, and N, their different combinations can result in the same Λ_e value [see Eq. (30)]. The figure here displays the analogies for four different Λ_e values, the latter spanning from Poisson ($\Lambda_e \to 0$) to Ch-GOE ($\Lambda_e \to \infty$) type spectral statistics. Each part of the figure displays the $P(r)$ behavior for different Ch-AEs, corresponding to four different combinations of e, w, and N (keeping w_s and t fixed) which keeps their Λ_e equal. The theoretical limits of Poisson ($\Lambda_e = 0$) and GOE ($\Lambda_e = \infty$) are also shown for comparison. The convergence of $P(r)$ for each case to the same curve and for all values of Λ_e lends support to our theoretical prediction about the latter being the only parameter governing the spectral fluctuations. The details of system and spectral parameters used here are given in Table I. The numerical results for $P(r)$ for each Λ value are also fitted with Eq. (29) with $\alpha(\beta_t) = \Lambda - 1.69\,(1-\beta_t) + 0.89\,(1-\beta_t)^5$ and the fitting parameters β_t and C_t given in Table I; for clarity, the fitted curves are not displayed here.

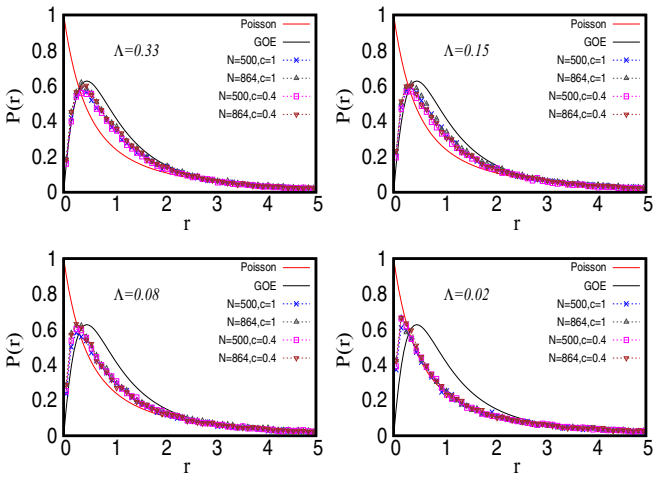

FIG. 4. Intrasystem analogy: nearest neighbor spacing ratio distribution for Ch-BE. The details here are the same as in Fig. 3 but now only two parameters, namely, c and N, are available to achieve same Λ_e value for different Ch-BEs. The details of system and spectral parameters used here are given in Table II.

as follows: we arbitrarily choose a set of system parameters, say s_1; numerically obtain the corresponding Ch-AE spectrum, say "AE1," by exact diagonalization and its $P(r)$ at an arbitrary spectral value, say $e = e_1$; find $R_1(e)$ and $\langle I_2 \rangle$ at e_1 from Figs. 1 and 2; and substitute them in Eq. (17) to obtain $\Lambda_e(e_1, s_1)$. The same procedure is then repeated to generate the Ch-AE spectrum, say "AE2" for the system parameter set s_2 again chosen arbitrarily, but the $P(r)$ for AE2 is numerically considered at an $e = e_2$ value (taking levels within $\leqslant 1\%$ of e_2) such that the equality $\Lambda_e(e_1, s_1) = \Lambda_e(e_2, s_2)$ is ensured. Note the latter condition limits the choice of s_2; it is arbitrary only to the extent that the relation $\Lambda_e(e_1, s_1) = \Lambda_e(e_2, s_2)$ can be satisfied within the available spectral range for the system. The same procedure is then repeated for the Ch-AEs with parameters s_3 and s_4.

As mentioned above, a variation of bulk statistics between two end points can only be seen if the ensemble is nonstationary. In the infinite N limit, the nonstationarity in AEs occurs only at some critical system parameter (e.g., critical disorder) or spectral point (e.g., mobility edge) [16,35], implying very few nonzero finite Λ_e values, which leaves very few options for satisfying Eq. (30). For finite system sizes, however, the AEs are known to have a critical regime of statistics different from Poisson and GOE or GUE and one can analyze the validity of Eq. (30) for many Λ_e values; here we consider the comparison for four different Λ_e values. To indicate that the statistics is indeed changing with Λ_e, the two stationary limits, namely, $P(r)$ for Poisson and GOE cases [Eqs. (27) and (28)], are also displayed in each part of the figure.

The system parameters for four Ch-AEs as well as the spectral parameters [i.e., $e, R_1(e)$, and $\langle I_2 \rangle$], used in Fig. 3 satisfying Eq. (30), are given in Table I. The eighth column of the latter gives the Λ_e values calculated from Eq. (17); here a small deviation can be seen due to unavailability of the exact analytical form of $R_1(e)$ and $\langle I_2(e) \rangle$, needed to invert $\Lambda_e(e_1, s_1)$ to find exact system parameters for other AEs. (Note column 1 of Table I mentions only the approximate Λ_e used as a label in Fig. 3.)

In contrast to Ch-AEs, with many system parameters, Ch-BEs, CH-PEs, and Ch-EEs depend only on one parameter besides matrix size N (see Sec. IV A). Figures 4–6 show $P(r)$ for four different Ch-BEs (obtained by changing μ, N, and e), Ch-PEs (different combinations of b and size N and e), and Ch-EEs (different combinations of b^2, N, and e), respectively. Here again the $P(r)$ analogies are obtained by repeating the same procedure as for Ch-AEs mentioned above [now Λ_e in Eq. (30) given by Eqs. (20), (23), and (26) for Ch-BE, Ch-PE, and Ch-EE, respectively]. The corresponding parametric values and spectral ranges leading to almost the same Λ_e values are given in Tables II, III, and IV (for Figs. 4, 5, and 6, respectively).

Note, for smaller Λ values, Figs. 3–6 may seem to indicate a different rate of crossover from Poisson to GOE. This may seem to suggest a violation of our theory which predicts statistical analogy if Λ_e is the same. We believe, however, this is due to numerical errors originating from (i) spectral averaging used in the numerics and (ii) lack of exact information about $R_1(e)$ and $\Delta_{\rm loc}(e)$. Also note $\Lambda_e(e)$ calculation is quite prone to errors for regions where $R_(e)$ changes rapidly, e.g., $e \sim 0$, as well as in the spectral-edge region and near inflection points for Ch-AE and Ch-PE (see Fig. 1).

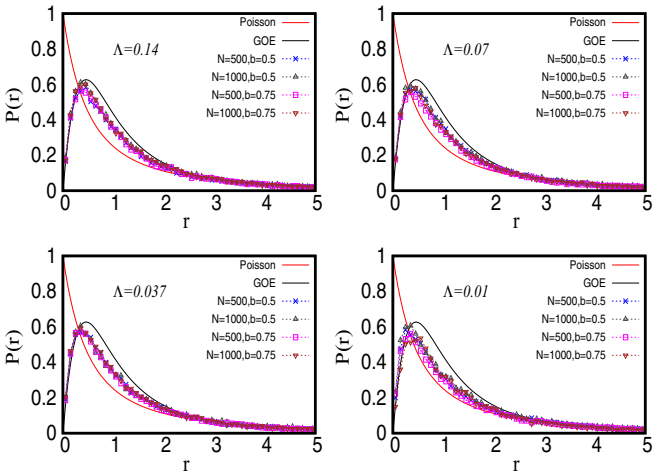

FIG. 5. Intrasystem analogy: nearest neighbor spacing ratio distribution for Ch-PE. The details here are the same as in Fig. 3 but again only two parameters, namely, b and N, are available to achieve same Λ_e value for different Ch-PEs. The details of system and spectral parameters used here are given in Table III.

Although not displayed in Figs. 3–6, we also fit $P(r)$ for each Λ with Eq. (29) with β_t and C_t as the fitting parameters and find $\alpha(\beta_t) = \Lambda - 1.69\,(1-\beta_t) + 0.89\,(1-\beta_t)^5$. The fitting parameters β_t and C_t for each case are given in Tables I–IV.

2. *Intersystem analogy*

In contrast to Ch-AEs, with many system parameters, Ch-BEs, CH-PEs, and Ch-EEs depend only on one parameter (besides matrix size N). It is therefore natural to query whether Eq. (31) can successfully be used to map their statistics onto each other. The condition for the ensemble and

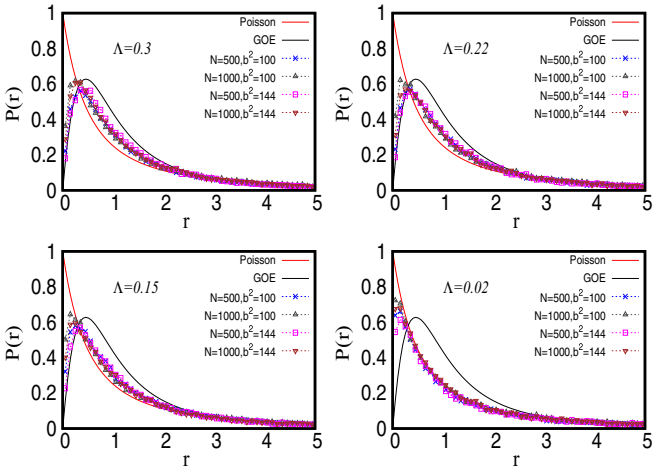

FIG. 6. Intrasystem analogy: nearest neighbor spacing ratio distribution for Ch-EE. The details here are the same as in Fig. 3 but again only two parameters, namely, b and N, are available to achieve same Λ_e value for different Ch-EEs. The details of system and spectral parameters used here are given in Table IV.

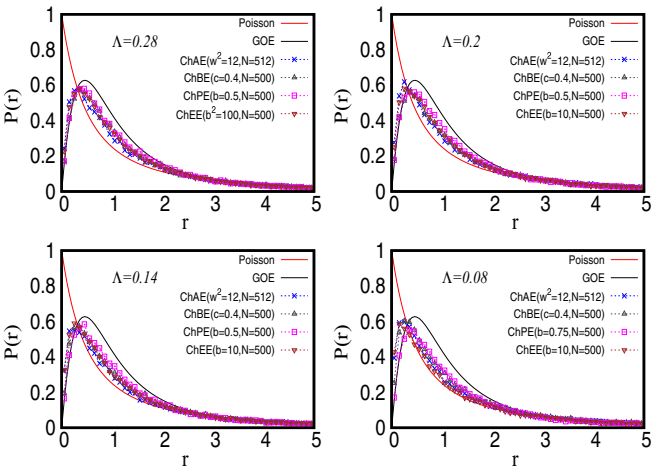

FIG. 7. Intersystem analogy: nearest neighbor spacing ratio distribution for $\beta = 1$. The figure displays the comparison of $P(r)$ for four different ensembles, namely, Ch-AE, Ch-BE, Ch-PE, and Ch-EE. Using Eqs. (17), (20), (23), and (26), respectively, the system parameters in each case are chosen such that they lead to the same Λ_e [see Eq. (31)]. A good convergence of $P(r)$ for each case to the same curve for large Λ and an almost convergence for small Λ once again confirm the insensitivity of the spectral fluctuations to microscopic system details. The details of system and spectral parameters used here are given in Table V.

spectral parameters leading to the analogs now becomes

$$\Lambda_{e,A}(s_1, e_1) = \Lambda_{e,B}(s_2, e_2) = \Lambda_{e,P}(s_3, e_3) = \Lambda_{e,E}(s_4, e_4) \tag{31}$$

with $\Lambda_{e,B}$, $\Lambda_{e,A}$, $\Lambda_{e,P}$, and $\Lambda_{e,E}$ given by Eqs. (20), (17), (23), and (26), respectively (with $\gamma = 1/4$). Here again the analogy is obtained by varying e values (note the analogy can also be studied for the same e values by a careful choice of ensemble parameters). As illustrated in Fig. 7, $P(r)$ for all the four cases with $\beta = 1$ overlap with each other if their Λ_e are equal. The details of each ensemble used in numerics for Fig. 7 are given in Table V. Although the overlap seems to be poor for small Λ values, this is again due to numerical errors associated with $\Delta_{\rm loc}(e)$ estimation (in contrast to intrasystem analogy, the error in the latter becomes crucial for comparisons of different systems). These errors can be reduced if an exact theoretical formulation of ξ is available for the system of interest. [Note that although $\xi \sim \langle I_2 \rangle^{-1}$ seems to work for Ch-AE and Ch-PE it is not an exact relation. Further, although intuitive reasoning in Sec. III B indicates that $\Delta_{\rm loc}(e) = \Delta(e)$ for RPE and $\Delta_{\rm loc}(e) = \sqrt{2N}\,\Delta(e)$ for Ch-EE are supported numerically, an exact formulation of $\Delta_{\rm loc}(e)$ for RPE and Ch-EE is still missing.]

We consider the intersystem analogy for $\beta = 2$ case too. The results are displayed in Fig. 8 along with Poisson and GUE limits; the parametric details for this figure are given in Table VI. [Although the figures for $R_1(e)$ and $\langle I_2(e) \rangle$ for the $\beta = 2$ case are not included in this paper, their values used for Λ_e calculation are given in Table VI.] The figure reconfirms our theoretical prediction regarding the insensitivity of local spectral statistics to specific system details and the role played by Λ_e.

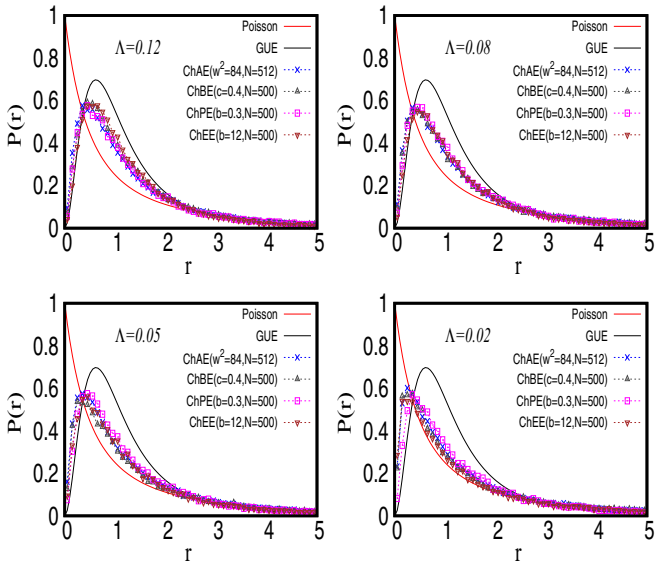

FIG. 8. Intersystem analogy: nearest neighbor spacing ratio distribution for $\beta = 2$. As in Fig. 7, here again we compare the four ensembles but now $P(r)$ for each case is analyzed for $\beta = 2$. The theoretical limits of Poisson ($\Lambda_e = 0$) and GUE ($\Lambda_e = \infty$) are also shown for comparison. The other details are the same as in Fig. 7 with details of system and spectral parameters used for this figure given in Table VI.

We fit $P(r)$ with Eq. (29) for all cases displayed in Figs. 7 and 8 and again find $\alpha(\beta_t) = \Lambda - 1.69\,(1-\beta_t) + 0.89\,(1-\beta_t)^5$ for $\beta = 1$ and $\alpha(\beta_t) = \Lambda - 1.42\,(2-\beta_t) + 0.01\,(2-\beta_t)^7 + 0.01\,(2-\beta_t)^6$ for $\beta = 2$. The fitting parameters β_t and C_t for each case are given in Tables V and VI.

V. CONCLUSION

In the end, we summarize with a brief discussion of our main results and open questions. Extending the complexity parameter formulation for Hermitian ensembles without chirality to those with chirality, we analyze, for the latter, the statistical response of the eigenvalues to multiparametric variations and its reduction to the complexity parameter formulation. As the chiral cases include non-Hermitian matrix blocks, this not only renders the technical analysis more complicated but also leads to the diffusion equations for the spectral JPDF different from the case without chirality. However, as in the nonchiral case, the spectral complexity parameter in the chiral case is again a function of energy as well as ensemble parameters. This predicts an important connection hidden underneath the local spectral fluctuations of a complex system: its statistics at an energy for a given set of system conditions can be analogous to that at another energy but with different system conditions. For two different complex systems, however, the analogy can occur even at the same energy if their complexity parameters are equal and both belong to the same global constraint class (i.e., same symmetry class and conservation laws). Our theoretical predictions are confirmed by a numerical comparison of the spectral statistics of four multiparametric Gaussian ensembles with different sets of ensemble parameters and at different energies.

Although, in the present paper, we have confined our analysis to spacing ratio distributions only (so as to minimize any error due to unfolding issues of the spectrum), previous studies on nonchiral ensembles have analyzed other measures too, e.g., nearest neighbor spacing distribution, number variance, etc. [16,18,20,27,36,38]; wave-function statistics [20]; and conductance distribution [37], etc.. These studies also support Λ_e based universality of the local fluctuations. As discussed in [24], the multiparametric chiral ensembles are connected to some other complex systems too, e.g., the systems represented by multiparametric Wishart ensembles and the CSH. The results and insights in the statistics of any one of them have therefore important implications for the others. Further, the appearance of Wishart matrices [23,39] in wide ranging areas makes the results derived for Chiral ensembles useful for these areas too. Considering that not many theoretical results so far are available for system-dependent random matrix ensembles (e.g., sparse ensembles of disordered Hamiltonians), the theoretical predictions based on complexity parametric formulation can be very useful and therefore need detailed investigations as well as experimental verifications if feasible.

Our paper still leaves many questions unanswered. The first and foremost among them is a theoretical formulation of $\Delta_{\rm local}(e)$ used in Eq. (11). Although we have given an intuitive reasoning in Sec. III B, its exact formulation is still missing. Further, the present paper is confined only to spectral statistics; a similar comparison for the eigenfunction fluctuations especially near zero energy is also very desirable (see [24] for more details). Another important question is about the transition from multiparametric chiral ensembles to nonchiral ensembles as chiral symmetry is partially broken. We intend to pursue some of these studies elsewhere.

APPENDIX A: SPECTRAL RESPONSE TO CHANGE IN SYSTEM CONDITIONS

As mentioned in Sec. III, the derivation of the diffusion equation for the eigenvalues in chiral cases, i.e., Eq. (9), is essentially similar to the nonchiral ones but their final responses turn out to be different. The difference arises from the response of the pairwise symmetric eigenvalues, chirality induced relations between eigenfunction components, as well as existence of zero modes in a chiral matrix. The chiral spectral responses needed to derive Eq. (9) (discussed in Appendix B) can be given as follows.

The eigenvalue equation for the matrix H can be given as $HU = \lambda U$ with λ as the diagonal matrix with eigenvalues λ_i of H as its matrix elements and U as the eigenvector matrix (unitary for the complex Hermitian case and orthogonal for the real-symmetric case).

Assuming the variation of system conditions leaves the chirality of H unaffected, the eigenvalues λ_{2N+k} for $k = 1 \to \nu$ therefore remain zero throughout the dynamics. The dynamics of λ_n, with $n = 1 \to N$, can then be given as

$$\frac{\partial \lambda_n}{\partial H_{k,N+l;s}} = i^{s-1}[U^*_{kn}U_{N+l,n} + (-1)^{s+1}U^*_{N+l,n}U_{kn}]. \quad \text{(A1)}$$

The above in turn gives

$$\sum_{k,l=1}^{N,N+\nu}\sum_{s=1}^{\beta}\frac{\partial\lambda_n}{\partial H_{k,N+l;s}}H_{k,N+l;s}=\lambda_n. \tag{A2}$$

Further,

$$\sum_{k,l=1}^{N,N+\nu}\sum_{s=1}^{\beta}\frac{\partial\lambda_n}{\partial H_{k,N+l;s}}\frac{\partial\lambda_m}{\partial H_{k,N+l;s}}=\beta\,\delta_{mn}\quad 1\leqslant m,n\leqslant N, \tag{A3}$$

$$\sum_{k,l=1}^{N,N+\nu}\sum_{s=1}^{\beta}\frac{\partial^2\lambda_n}{\partial H_{k,N+l;s}^2}=\frac{\beta(\nu+1/2)}{\lambda_n}+\sum_{m=1\neq n}^{N}\frac{2\,\beta\,\lambda_n}{\lambda_n^2-\lambda_m^2}. \tag{A4}$$

By replacing the subscript n by $N+n$, the above equations can directly be used to derive the response for the negative eigenvalues λ_{n+N}. Note in this context that chirality leads to the condition $U_{N+l,N+n}=-U_{N+l,n}$ and, consequently, the replacement of $\lambda_n\to-\lambda_{N+n}$ leaves Eqs. (A1)–(A4) invariant.

As discussed in Appendix B, the above relations lead to Eq. (9), essentially following the same steps as used in [15,17] for the nonchiral case.

APPENDIX B: DERIVATION OF EQ. (9)

The probability density $P_N(E,Y)$ of finding positive eigenvalues λ_i between e_i and e_i+de_i at a given Y can be expressed in terms of the matrix elements distribution:

$$P_N(E,Y)=\int\prod_{i=1}^{N}\delta(e_i-\lambda_i)\,\delta(e_i+\lambda_{N+i})\,\rho(H,Y)\,dH. \tag{B1}$$

Here E refers to a diagonal matrix with elements $e_1,\ldots,e_n$. As the Y dependence of P_N in Eq. (B1) enters only through ρ, a derivative of P_N with respect to Y can be written as follows:

$$\frac{\partial P_N}{\partial Y}=\int\prod_{i=1}^{N}\delta(e_i-\lambda_i)\,\delta(e_i+\lambda_{N+i})\,\frac{\partial\rho}{\partial Y}dH. \tag{B2}$$

Substitution of Eq. (7) in Eq. (B2) leads to

$$\frac{\partial P_N}{\partial Y}=I_1+I_2 \tag{B3}$$

where

$$I_1=\gamma\sum_{\mu}\int\prod_{i=1}^{N}\delta(e_i-\lambda_i)\,\delta(e_i+\lambda_{N+i})\,\frac{\partial(H_\mu\,\rho)}{\partial H_\mu}\,dH, \tag{B4}$$

$$I_2=\sum_{\mu}\int\prod_{i=1}^{N}\delta(e_i-\lambda_i)\,\delta(e_i+\lambda_{N+i})\,\frac{\partial^2\rho}{\partial H_\mu^2}\,dH \tag{B5}$$

with $H_\mu\equiv H_{k,N+l;s}$ with $1\leqslant k,l\leqslant N$. I_1 can further be simplified by integration by parts:

$$I_1=-\gamma\sum_{\mu}\int\frac{\partial}{\partial H_\mu}\left[\prod_{i=1}^{N}\delta(e_i-\lambda_i)\,\delta(e_i+\lambda_{N+i})\right]H_\mu\,\rho\,dH \tag{B6}$$

$$=2\,\gamma\sum_{n=1}^{N}\frac{\partial}{\partial e_n}\int\prod_{i=1}^{N}\delta(e_i-\lambda_i)\,\delta(e_i+\lambda_{N+i})\left[\sum_{\mu}\frac{\partial\lambda_n}{\partial H_\mu}H_\mu\right]\rho\,dH. \tag{B7}$$

Here the second equality follows from the relations (i) $\frac{\partial\delta(e_n-\lambda_n)}{\partial H_\mu}=\frac{\partial\delta(e_n-\lambda_n)}{\partial e_n}\frac{\partial\lambda_n}{\partial H_\mu}$ and (ii) $\frac{\partial\delta(e_n+\lambda_{N+n})}{\partial H_\mu}=-\frac{\partial\delta(e_n+\lambda_{N+n})}{\partial e_n}\frac{\partial\lambda_{N+n}}{\partial H_\mu}=\frac{\partial\delta(e_n+\lambda_{N+n})}{\partial e_n}\frac{\partial\lambda_n}{\partial H_\mu}$. Now using Eq. (A2) of Appendix A in Eq. (B7), we have

$$I_1=2\gamma\sum_{n}\frac{\partial}{\partial e_n}(e_nP_N). \tag{B8}$$

I_2 can similarly be reduced as follows:

$$I_2=\sum_{\mu}\int\frac{\partial^2}{\partial H_\mu^2}\left[\prod_{i}\delta(e_i-\lambda_i)\,\delta(e_i+\lambda_{N+i})\right]\rho\,dH \tag{B9}$$

$$=2\sum_{m,n}\frac{\partial^2}{\partial e_n\partial e_m}\int\prod_{i}\delta(e_i-\lambda_i)\,\delta(e_i+\lambda_{N+i})\left[\sum_{\mu}\frac{\partial\lambda_m}{\partial H_\mu}\frac{\partial\lambda_n}{\partial H_\mu}\right]\rho\,dH$$

$$-2\sum_{m}\frac{\partial}{\partial e_n}\int\prod_{i}\delta(e_i-\lambda_i)\,\delta(e_i+\lambda_{N+i})\left[\sum_{\mu}\frac{\partial^2\lambda_n}{\partial H_\mu^2}\right]\rho\,dH. \tag{B10}$$

Further, using Eqs. (A3) and (A4), I_2 can be expressed in terms of eigenvalue derivatives of ρ:

$$I_2=2\sum_{n=1}^{N}\frac{\partial}{\partial e_n}\left[\frac{\partial}{\partial e_n}-\frac{(\nu+1/2)\beta}{e_n}-\sum_{m=1}^{N}\frac{2\beta e_n}{e_n^2-e_m^2}\right]P_N. \tag{B11}$$

A substitution of I_1 and I_2 in Eq. (B3) leads to Eq. (9), describing the single parametric evolution of the eigenvalues of the ensemble $\rho(H)$.

[1] A. Altland and M. R. Zirnbauer, Phys. Rev. B **55**, 1142 (1997).
[2] P. Shukla, Int. J. Mod. Phys. B **26**, 1230008 (2012).
[3] F. Dyson, J. Math. Phys. **3**, 1191 (1962).
[4] F. Haake, *Quantum Signatures of Chaos* (Springer-Verlag, Berlin, 1991).
[5] M. L. Mehta, *Random Matrices* (Academic, New York, 1991).
[6] T. Guhr, G. A. Muller-Groeling, and H. A. Weidenmuller, Phys. Rep. **299**, 189 (1998).
[7] A. Ferreira and E. R. Mucciolo, Phys. Rev. Lett. **115**, 106601 (2015); A. Cresti, F. Ortmann, T. Louvet, Dinh Van Tuan, and S. Roche, Phys. Rev. Lett **110**, 196601 (2013); L. Liu, Y. Yu, H. B. Wu, Y.-Y. Zhang, J.-J. Liu, and S. S. Li, Phys. Rev. B **97**, 155302 (2018); N. Weik, J. Schindler, S. Bera, G. C. Solomon, and F. Evers, *ibid.* **94**, 064204 (2016); G. Santhosh, V. Sreenath, A. Lakshminarayan, and R. Narayanan, *ibid.* **85**, 054204 (2012); N. M. R. Peres, S.-W. Tsai, J. E. Santos, and R. M. Ribeiro, *ibid.* **79**, 155442 (2009).
[8] J. J. M. Verbaarschot, Phys. Rev. Lett. **72**, 2531 (1994); Nucl. Phys. B **53**, 88 (1997); T. Wettig, A. Schafer, and H. A. Weidenmuller, Nucl. Phys. A **610**, 492 (1996); J. J. M. Verbaarschot and T. Wettig, Annu. Rev. Nucl. Part. Sci. **50**, 343 (2000).
[9] R. Gade, Nucl. Phys. B **398**, 499 (1993).
[10] K. Slevin and T. Nagao, Phys. Rev. Lett. **70**, 635 (1993).
[11] C. W. J. Beenakker, Rev. Mod. Phys. **87**, 1037 (2015).
[12] V. Gurarie and J. T. Chalker, Phys. Rev. B **68**, 134207 (2003).
[13] S. N. Evangelou and D. E. Katsanos, J. Phys. A: Math. Gen. **36**, 3237 (2003).
[14] H. Schomerus, M. Marciani, and C. W. J. Beenakker, Phys. Rev. Lett. **114**, 166803 (2015).
[15] P. Shukla, Phys. Rev. E **62**, 2098 (2000).
[16] P. Shukla, J. Phys.: Condens. Matter **17**, 1653 (2005).
[17] P. Shukla, Phys. Rev. E **71**, 026226 (2005).
[18] R. Dutta and P. Shukla, Phys. Rev. E **76**, 051124 (2007).
[19] P. Shukla, J. Phys. A: Math. Theor. **41**, 304023 (2008).
[20] P. Shukla, Phys. Rev. E **75**, 051113 (2007).
[21] S. Sadhukhan and P. Shukla, Phys. Rev. E **96**, 012109 (2017).
[22] J. B. French, V. K. B. Kota, A. Pandey, and S. Tomsovic, Ann. Phys. (NY) **181**, 235 (1988).
[23] S. Kumar and A. Pandey, Ann. Phys. (NY) **326**, 1877 (2011); Phys. Rev. E **79**, 026211 (2009).
[24] P. Shukla, arXiv:2004.14860.
[25] P. Shukla, AIP Conf. Proc. **553**, 215 (2001).
[26] E. Cuevas and V. E. Kravtsov, Phys. Rev. B **76**, 235119 (2007).
[27] P. Shukla, Phys. Rev. B **98**, 054206 (2018); **98**, 184202 (2018).
[28] P. Shukla, New J. Phys. **18**, 021004 (2016).
[29] A. D. Mirlin, Y. V. Fyodorov, F. M. Dittes, J. Quezada, and T. H. Seligman, Phys. Rev. E **54**, 3221 (1996).
[30] The subroutines used for diagonalization of complex matrices are available at www.netlib.org.
[31] V. Oganesyan and D. A. Huse, Phys. Rev. B **75**, 155111 (2007).
[32] Y. Y. Atas, E. Bogomolny, O. Giraud, and G. Roux, Phys. Rev. Lett. **110**, 084101 (2013).
[33] Á. L. Corps and A. Relano, Phys. Rev. E **101**, 022222 (2020).
[34] B. Shapiro, Int. J. Mod. Phys. B **10**, 3539 (1996).
[35] Antonio M. García-García and K. Takahashi, Nucl. Phys. B **700**, 361 (2004).
[36] R. Dutta and P. Shukla, Phys. Rev. E **78**, 031115 (2008).
[37] A. Pandey and P. Shukla, J. Phys. A **24**, 3907 (1991).
[38] D. Dey and P. Shukla, Phys. Rev. E **90**, 052118 (2014).
[39] P. Shukla, J. Phys. A: Math. Theor. **50**, 435003 (2017).